Current transport mechanism in trapped oxides: A generalized trap-assisted tunneling model

Mau Phon Houng, Yeong Her Wang, and Wai Jyh Chang
Department of Electrical Engineering, National Cheng-Kung University, Tainan, Taiwan, Republic of China

(Received 4 December 1998; accepted for publication 20 April 1999)

A generalized trap-assisted tunneling (GTAT) model is proposed in this work, where an effective tunneling barrier of trapezoidal shape is considered, instead of the triangular barrier utilized in the conventional trap-assisted tunneling (TAT) model. It is demonstrated that trapezoidal barrier tunneling dominates at low electric fields ($E<4$ MV/cm), while triangular barrier tunneling contributes the main part of the tunneling current at high electric fields ($E=6-8$ MV/cm). The comparisons of this improved model and the results of the conventional TAT model at high and low electric fields are discussed. It is concluded that GTAT can more accurately model the current density-electric field ($J-E$) curves for the conduction enhancement of a trapped oxide film under various deposition conditions over a wider range of electric fields. This is confirmed by the comparative use of both TAT and GTAT models on experimental data obtained from existing reports. Furthermore, a simple method for determining the trap energy level is derived from the $J-E$ relationship. This method provides a convenient way to characterize the trap levels inside the oxide layers, without the need of other complicated measurements. The developed GTAT model can be applied to the investigations of gate oxide reliability, especially the stress-related effects and impurity incorporated oxide films (i.e., SiOF or SiON). © *1999 American Institute of Physics.* [S0021-8979(99)01615-1]

I. INTRODUCTION

The electrical conduction mechanisms of thin trapped silicon oxide films have attracted much attention over many years.[1–6] In the literature it is found that the enhanced conductivity of intentionally doped thermal oxide (i.e., nitrided silicon oxide) and stress-induced-leakage current (SILC) could be well described by the trap model. Suzuki *et al.*[4] proposed a model involving two-step tunneling via traps [hereafter, trap-assisted tunneling (TAT)] to explain the current enhancement in nitrided oxides. Two unique phenomena have been found from the modeling of experimental data: after nitridation, the effective barrier height for tunneling electrons is lowered (from 3.1 to 2.5 eV); a high density of deep traps is created. However, the subsequent investigators, Cheng *et al.*[5] and Fleischer *et al.*,[6] gave an alternative form of the TAT model to describe the effect of heavy nitridaiton on current enhancement, and also simplified the TAT model to an analytical form. Cheng's and Fleischer's TAT models were based on a triangular barrier for tunneling electrons and a deep level of nitridation generated traps below the oxide conduction band. Real electron tunneling behavior remains unclear, and these theoretical assumptions may not be true. Moreover, their models can describe only a partial range of the current density-electric field ($J-E$) characteristics (i.e., a high electric field of 6–8 MV/cm). In this article, we propose a generalized trap-assisted tunneling (GTAT) model to characterize the $J-E$ curves under various bias conditions. Furthermore, we present a convenient way to derive Φ_t (that is, trap energy level below the oxide conduction band) directly from the $J-E$ curve, without capacitance–voltage ($C-V$) or deep level transient spectroscopy (DLTS) measurements.

II. IMPROVEMENT OF THE TAT MODEL

Following the TAT model given by Cheng *et al.*,[5] the energy band diagram of a biased Al–SiO_2–Si structure is in the form of triangular barrier. When electrons exist in the metal–oxide interface, they tunnel through this insulating layer. However, it is recognized that a trapezoidal barrier and not a triangular barrier exist in the interface. A trapezoidal barrier contributes additional tunneling paths and dominates the tunneling current at low electric fields.

Figure 1 shows the energy band diagram of the proposed GTAT model for electrons tunneling from metal to the conduction band of the oxide layer. Two cases are considered in which the generated traps exist: (i) at a shallow level [$\Phi_t > \Phi_B$, Fig. 1(a)] and (ii) at a deep level [$\Phi_t < \Phi_B$, Fig. 1(b)]. The symbols used in this figure are listed in the following: Φ_B is the barrier height of Fowler–Nordheim (F–N) tunneling, Φ_t is the trap energy below the oxide conduction band, Φ is the potential barrier of a tunneling electron measured from electron energy to the oxide conduction band, which is not shown in this figure, P_1 and P_2 refer to the tunneling probability for electrons tunneling into traps and, subsequently, tunneling into silicon, respectively. V is the applied voltage, and T_{ox} is the oxide thickness.

Under the condition of $\Phi_t > \Phi_B$ in Fig. 1(a), when the applied voltage is sufficiently high, electrons tunneling from metal to oxide can meet either a triangular shape [tunneling process A in Fig. 1(a)] or a trapezoidal shape [tunneling process B in Fig. 1(a)] depending on the potential barrier Φ. Thus, we can start GTAT calculation by using the Wentzel–Kramers–Brillouin (WKB) approximation[7] for the tunneling probability, P_1 and P_2:

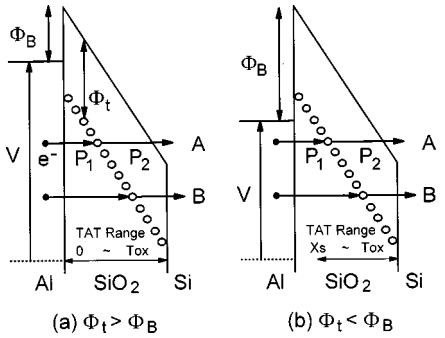

FIG. 1. Schematic energy band diagram of an Al–SiO_2–Si structure under a negative bias: (a) $\Phi_t > \Phi_B$ and (b) $\Phi_t < \Phi_B$. The tunneling barrier is either triangular (process A) or trapezoidal (process B) depending on the potential barrier (Φ) of an electron. Note that the ideal Φ_B is 3.2 eV for both two cases in this figure.

$$P_i = \exp\left(-2 \int |k(x)| dx \right) \quad i = 1 \text{ or } 2, \tag{1}$$

and $k(x)$ is given by

$$k(x) = \left[\frac{2qm_{\text{ox}}}{\hbar^2} (\Phi_B - Ex - E_e) \right]^{1/2}, \tag{2}$$

where m_{ox} is the effective mass of the electron in oxide, E is the electric field across the oxide, and E_e is the total electron energy in metal (taken as 0.2 eV[8]). By integrating $k(x)$ and substituting suitable boundary conditions, we can get P in the form of:

$$P_i = \exp \frac{-4\sqrt{2qm_{\text{ox}}}}{3\hbar E} (\Psi_i^{3/2} - \psi_i^{3/2}) \quad i = 1 \text{ or } 2. \tag{3}$$

Here, determination of Ψ and ψ depends on which barrier the electron tunnels through:

(i) Triangular barrier (tunneling process A in Fig. 1)

$$\Psi_1 = \Phi(x); \quad \psi_1 = \Phi_t,$$

$$\Psi_2 = \Phi_t; \quad \psi_2 = 0,$$

(ii) Trapezoidal barrier (tunneling process B in Fig. 1)

$$\Psi_1 = \Phi(x); \quad \psi_1 = \Phi_t,$$

$$\Psi_2 = \Phi_t; \quad \psi_2 = \Phi(x) - V,$$

and $\Phi(x) = \Phi_t + Ex - E_e$. Therefore, the tunneling current J_t can be calculated by:

$$J_t = \int \frac{qC_t N_t P_1 P_2}{P_1 + P_2} dx, \tag{4}$$

where C_t is a function of Φ_t and E_e (see Ref. 6) and N_t is the trap concentration. Apparently, from Fig. 1, the integration range of $k(x)$ is $(0 - T_{\text{ox}})$ for $\Phi_t > \Phi_B$ and $(X_s - T_{\text{ox}})$ for $\Phi_t < \Phi_B$, where $X_s = (\Phi_B - \Phi_t - E_e)/E$. The two integration ranges are essentially the same, with the exception that when $\Phi_t < \Phi_B$, the effective TAT range is somewhat smaller [see Fig. 1(b)].

In the GTAT model, the tunneling current can be classified into two parts:

$$J_t = J_{\text{tri}} + J_{\text{tra}}, \tag{5}$$

where J_{tri} is the tunneling current through the triangular barrier and J_{tra} is the tunneling current through the trapezoidal barrier, respectively. With the assumption of $\Phi_t + Ex \gg E_e$, the analytical expressions of J_{tri} and J_{tra} can be obtained as follows:

$$J_{\text{tri}} = C_1 \exp\left(-\frac{C_2}{E} \right) \left\{ \left(C_3 - \frac{3C_2}{2E} \right) - \ln\left[\frac{1 + \exp(C_3 - 5C_2/2E)}{1 + \exp(-C_2/E)} \right] \right\}, \tag{6}$$

where

$$C_1 = \frac{2qC_t N_t}{3A\sqrt{\Phi_t}},$$

$$C_2 = \Phi_t^{3/2} A, \quad \text{for } \Phi_t > \Phi_B,$$

$$C_2 = \frac{1}{2} A \sqrt{\Phi_t} (5\Phi_t - 3\Phi_B) \quad \text{for } \Phi_t < \Phi_B,$$

$$C_3 = \frac{3}{2} A T_{\text{ox}} \sqrt{\Phi_t},$$

$$A = \frac{4\sqrt{2qm_{\text{ox}}}}{3\hbar},$$

and

$$J_{\text{tra}} = -C_1 R_1 \left\{ \tan^{-1}\left(\frac{R_2}{R_1} \right) - \tan^{-1}\left[\frac{\exp(-C_3 + 3\Phi_t^{3/2}/2E)}{R_1} \right] \right\}, \tag{7}$$

where $R_1 = \exp(-C_3/2)$ and $R_2 = \exp(C_3)$ for both $\Phi_t > \Phi_B$ and $\Phi_t < \Phi_B$. From Eqs. (6) and (7), it may be found that J_{tri} dominates at high electric fields ($E > 6$ MV/cm) while J_{tra} is the major current at low electric fields. When a high electric field is applied, the tunneling current predicted by GTAT is almost the same as that of the TAT model. However, an additional tunneling current at low electric field levels, disregarded by TAT, is predicted by GTAT.

In order to give a qualitative analysis of J and E, the current–voltage relationship at high electric fields ($E > 6$ MV/cm and $J_{\text{tri}} \gg J_{\text{tra}}$) is expressed as

$$J_t \sim \exp\left(-\frac{4\sqrt{2qm_{\text{ox}}}}{3\hbar} \Phi_t^{3/2}/E \right). \tag{8}$$

From this simple approximation, it is easy to determine Φ_t by plotting $\ln J$ vs $1/E$ (i.e., the TAT plot) and measuring the slope of this curve. By deriving Φ_t as a first step, the fitting procedure can be expected to be easier and more accurate. Figure 2 shows an example of a TAT plot with experimental data from Fleischer *et al.*[6] At electric field of 6–8 MV/cm, as indicated in Fig. 2, the experimental data reveals a straight line with a corresponding value of $\Phi_t = 2.62$ eV [by Eq. (8)]. This value is very close to the fitting value of 2.63 eV. It

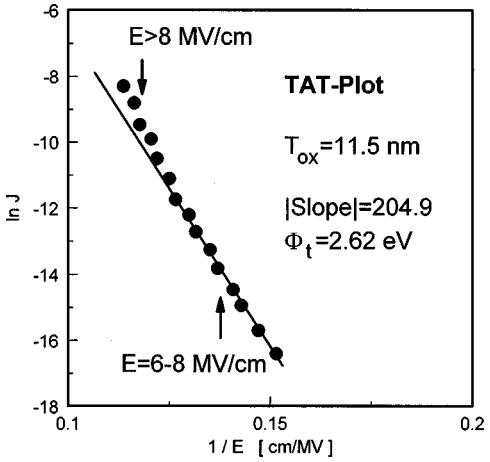

FIG. 2. A TAT-plot schematic of a nitrided thermal oxide with oxide thickness 11.5 nm. The linear region at low electric fields represents a trap-assisted tunneling mechanism. The trap energy can be derived from the curve slope and Eq. (8).

therefore confirms that this method can greatly simplify the derivation of Φ_t by use of only a $J-E$ curve.

III. RESULTS AND DISCUSSION

Figure 3 shows a comparison of experimental and theoretical curves for the tunneling current at both low and high electric fields. At low fields, the data is from Suzuki *et al.*,[4] NH_3 nitrided at 1000 °C for 60 min, while at high fields, the data is from Fleischer *et al.*,[6] nitrided at an ammonia:nitrogen=1:20 dilution for 15 min at 950 °C. Results predicted by TAT and GTAT models are shown for comparison.

The investigation by Fleischer *et al.*[6] assumes $\Phi_t > \Phi_B$ [see Fig. 1(a)] and a triangular tunneling barrier, and successfully models the conduction mechanism at electric fields of 6–8 MV/cm via the TAT model. It is also clear that F–N tunneling dominates at $E>8$ MV/cm. From Fig. 3, it is revealed that both TAT and GTAT can give good fits of experimental data at electric fields of 6–8 MV/cm. However, within the 6–8 MV/cm range, the conventional TAT model is based on some physically unrealistic premises. For the TAT model, Φ_t is assumed to be larger than Φ_B, which is a questionable assumption. F–N plotting indicates $\Phi_B = 2.83\,\text{eV}$, which is larger than Fleischer's proposed value of $\Phi_t = 2.1\,\text{eV}$ [case (a) in Fig. 1]. From another work, also by Fleischer *et al.*,[9] using $\Phi_t = 0.7\,\text{eV}$ and $N_t = 5\times10^{20}\,\text{cm}^{-3}$, the TAT model gives a reasonable fit to the nitrided data, but this value of Φ_t is too small for a reasonable Φ_B in their assumption. Via the TAT model, reasonable values of Φ_t fail to yield a good experimental fit for $\Phi_t < \Phi_B$, and thus an improved TAT model must be considered. Figure 3 shows that, using the GTAT model and a much more reasonable value of $\Phi_t = 2.63\,\text{eV}$ to generate a $J-E$ curve, values of $\Phi_t < \Phi_B$ give a good fit of the experimental data. Also in Fig. 3, the same fitting parameters are used to calculate the $J-E$ curve for the TAT model. The fitting parameters Φ_t and N_t for the TAT curve are slightly changed in order to create a visible difference between the two virtually identical curves. The similarity of these two curves is due to the electric field being high enough that the TAT integration range is almost the same ($X_s \approx 0$), and the contribution of trapezoidal barrier tunneling being reduced at this electric field range.

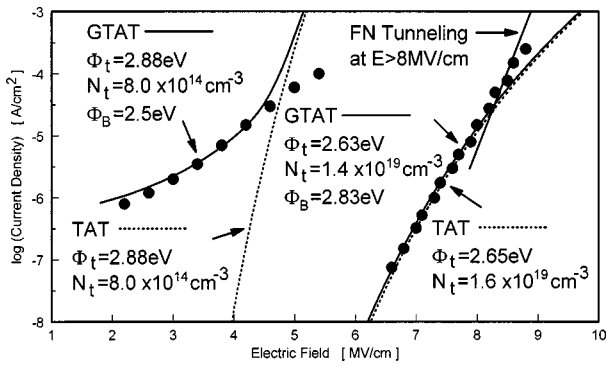

FIG. 3. Comparison of experimental and fitting curves for GTAT and TAT models for tunneling current at high and low electric fields. The dotted data at a low electric field are from Suzuki *et al.* (see Ref. 4) with an oxide thickness of 7.4 nm while the dotted data at a high electric field are from Fleischer *et al.* (see Ref. 6) with an oxide thickness of 11.5 nm. Furthermore, it is shown that Fowler–Nordheim tunneling dominates at $E>8$ MV/cm (solid straight line).

For low electric fields (2–5 MV/cm), given data as presented by Suzuki *et al.*,[4] obviously dissimilar $J-E$ curves are obtained from the TAT and GTAT models. If the TAT model is utilized, no suitable $J-E$ curve can be found to fit the experimental data. However, the GTAT model can provide a reasonable fit at low electric fields (less than 5 MV/cm) with $\Phi_t = 2.88\,\text{eV}$ and $N_t = 8\times10^{14}\,\text{cm}^{-3}$. At higher electric fields of 4.5–5.5 MV/cm, it is found that the experimental data diverges from the calculated curve. One can also find that at this field range, the slope of the calculated curve is the same as the one at $E=6-8$ MV/cm, indicating that J_{tri} dominates at this field range. The GTAT model gives the $J-E$ curve with over-predicted tunneling current by comparing with the experimental data. Suzuki's TAT results showed a similar divergence and suggested that this was due to a lack of traps contributing to a low tunneling probability.[4] Furthermore, they found that the tunneling current at $E=4.5-5.5$ MV/cm can be modeled by assuming no traps existed in the oxide film. We believe the distribution of most of the traps were close to the oxide/Si interface so that the direct tunneling instead of triangular tunneling should be considered. From the fitting curves shown in Fig. 3, at low electric fields, it is clear that a very different tunneling behavior is observed. That is, for the same Φ_t and N_t, the TAT model gives a steep $J-E$ curve over the whole low electric field region whereas the GTAT model gives a large tunneling current at $E=2-4$ MV/cm. The reason is explained as follows. As can be seen in Fig. 1, the GTAT model takes into account a general case of electron tunneling behaviors. At low electric fields, the lowering of the oxide conduction band decreases so that the contribution of triangular barrier tunneling is suppressed. If the TAT model is used to explain the conduction mechanism, only triangular barrier tunneling is considered and hence the additional tunneling path via the trapezoidal barrier is ignored. Figure 3 shows that trapezoidal barrier tunneling dominates at low electric fields. For calcu-

lating tunneling current in the low electric field range, the GTAT model is demonstrated to be able to accurately model the experimentally derived $J-E$ curves.

IV. CONCLUSION

A generalized TAT model is proposed in this article to solve some of the problems met with the conventional TAT model. Compared to the conventional TAT model, which only considers $\Phi_t > \Phi_B$ and triangular barriers, GTAT considers the more general case of $\Phi_t > \Phi_B$ and $\Phi_t < \Phi_B$, which includes both triangular and trapezoidal barrier tunneling. It is concluded that GTAT can accurately model $J-E$ curves for a wider range of electric fields than TAT. This is confirmed by the comparative use of both TAT and GTAT models on experimental data obtained from existing reports. This new model can also be used to explain the current enhancement of fluorinated silicon oxide (SiOF) or stress-induced-leakage current in an ultrathin thermal oxide. Furthermore, a simple method is offered for deriving the trap energy level in a trapped oxide, and is demonstrated to be an accurate parameter extraction method, without the complications of previous methods.

ACKNOWLEDGMENT

This work was partially supported by the National Science Council of Republic of China under Contract No. NSC 88-2215-E-006-007.

[1] B. Ricco, G. Gozzi, and M. Lanzoni, IEEE Trans. Electron Devices **45**, 1554 (1998).
[2] A. I. Chou, K. Lai, K. Kumar, P. Chowdhury, and J. C. Lee, Appl. Phys. Lett. **70**, 3407 (1997).
[3] K. Okada and K. Taniguchi, Appl. Phys. Lett. **70**, 351 (1997).
[4] E. Suzuki and D. K. Schroder, J. Appl. Phys. **60**, 3616 (1986).
[5] X. R. Cheng, Y. C. Cheng, and B. Y. Liu, J. Appl. Phys. **63**, 797 (1988).
[6] S. Fleischer, P. T. Lai, and Y. C. Cheng, J. Appl. Phys. **72**, 5711 (1992).
[7] S. J. Oh and Y. T. Yeow, Solid-State Electron. **32**, 507 (1989).
[8] C. Svensson and I. Lundstrom, J. Appl. Phys. **44**, 4657 (1973).
[9] S. Fleischer, P. T. Lai, and Y. C. Cheng, J. Appl. Phys. **73**, 8353 (1993).